



Growth, collapse, and stalling in a mechanical model for neurite motility

Pierre Recho,^{1,*} Antoine Jerusalem,^{2,†} and Alain Goriely^{1,‡}

¹*Mathematical Institute, University of Oxford, Oxford OX26GG, United Kingdom*

²*Department of Engineering Science, University of Oxford, Oxford OX13PJ, United Kingdom*

(Received 28 November 2015; published 18 March 2016)

Neurites, the long cellular protrusions that form the routes of the neuronal network, are capable of actively extending during early morphogenesis or regenerating after trauma. To perform this task, they rely on their cytoskeleton for mechanical support. In this paper, we present a three-component active gel model that describes neurites in the three robust mechanical states observed experimentally: collapsed, static, and motile. These states arise from an interplay between the physical forces driven by growth of the microtubule-rich inner core of the neurite and the acto-myosin contractility of its surrounding cortical membrane. In particular, static states appear as a mechanical traction or compression balance of these two parallel structures. The model predicts how the response of a neurite to a towing force depends on the force magnitude and recovers the response of neurites to several drug treatments that modulate the cytoskeleton active and passive properties.

DOI: [10.1103/PhysRevE.93.032410](https://doi.org/10.1103/PhysRevE.93.032410)

I. INTRODUCTION

Neurons are cells with long and thin ($\sim 1 \mu\text{m}$ in diameter) quasi-one-dimensional processes called neurites, a term that comprises the axon, which emits electric signals, and dendrites, which are generally shorter and receive signals. These processes emerge from the cell body (the *soma*), and, during embryonic development or regeneration after a trauma, they are able to crawl over large distances to reach targets from other neurons, thus forming a complex nervous network essential for both perception and motion. Understanding how neurites can establish these long-distance connections is a problem that was pioneered more than a century ago [1] and is of paramount therapeutic importance. For instance, injuries of the spinal cord are often characterized by an irreversible and debilitating loss of motor and sensory functions of the lower body (paraplegia, tetraplegia) because disrupted neurites cannot overcome the inflammation and are incapable of initiating extensions that would rebuild the broken connections [2–4].

The cytoskeleton of neurites is the mechanical scaffold that maintains their morphology and motility [5–8]. Extrinsic and intrinsic guidance clues may be viewed as agents that influence the physical state of the cytoskeleton via biochemical pathways [9–12]. For example, the concentration of calcium is known to influence the Rho pathway, which in turn modulates the neurite contractility and can lead to a reversible collapse that shortens the axon [13].

The neuronal cytoskeleton (see Ref. [8] for an extensive review and Fig. 1 for a simplified scheme) is a meshwork of three main types of biological polymers: F-actin, microtubules, and neurofilaments, all of which contribute mechanically [14]. While neurofilaments are passive and apolar, both F-actin and microtubules are capable of polymerizing at one end (with the addition of G-actin and tubulin subunits, respectively) and depolymerizing at the other (by the removal of subunits) with potentially low (~ 1 min) turnover duration. They can

also both be cross-linked by molecular motors (myosin II for F-actin, dynein, or kinesin for microtubules) that are able to exert active stresses inside the meshwork [15–17]. Following Ref. [5], we define two different compartments of the neurite where the cytoskeleton is organized in a different way: the *kinetoplasm*, or growth cone (GC), at the proximal end of the neurite, and the *axoplasm*, which connects the GC to the soma. The axoplasm contains a core array of para-axial microtubules connected by passive cross-linkers [microtubules associated proteins (MAP)] that generate a network with a quasilattice structure [18]. These microtubules are highly stable (turnover duration of hours) possibly due to the presence of MAPs. In the axoplasm, F-actin is mostly organized into a cortical mesh around the microtubule's inner core and the presence of myosin II motors in this cortex lead to the presence of contractile stresses [19]. These two meshworks are physically connected by different types of special proteins (such as +TIP; see Ref. [8]) that mediate force transmission between them. In continuity with this cortex, the GC is almost free of microtubules, apart from those engaging into filopodia, while F-actin is organized in a lamellipodium similar to the ones found in cells specialized in crawling (such as keratocytes [20]). Filaments polymerizing at the leading edge (the *P-domain*) protrude from the membrane and are then advected backward by a retrograde flow powered by myosin II motors that concentrate at the trailing edge of the GC (the *T-domain*) [21]. Actin then accumulates into thick bundles in the T-domain, which constitutes the main obstacle preventing microtubules from entering the GC. The cytoskeleton is connected to the external substrate/cellular matrix by special proteins specialized in adhesion, such as integrins and cadherins [22,23].

Numerous authors have proposed physical models to explain how the neurite cytoskeleton drives its motility [7,25–27]. These models can be divided into two main classes depending on whether they imply that the GC pulls the trailing axoplasm thanks to F-actin polymerization pushing the membrane in the P-domain [28,29] and myosin II contractility pulling from the T-domain [30–33], or whether it is instead microtubules that, from the axoplasm, polymerize against the T-domain and propel the GC [34,35], or both [36]. As the

*pierre.recho@polytechnique.edu

†antoine.jerusalem@eng.ox.ac.uk

‡goriely@maths.ox.ac.uk

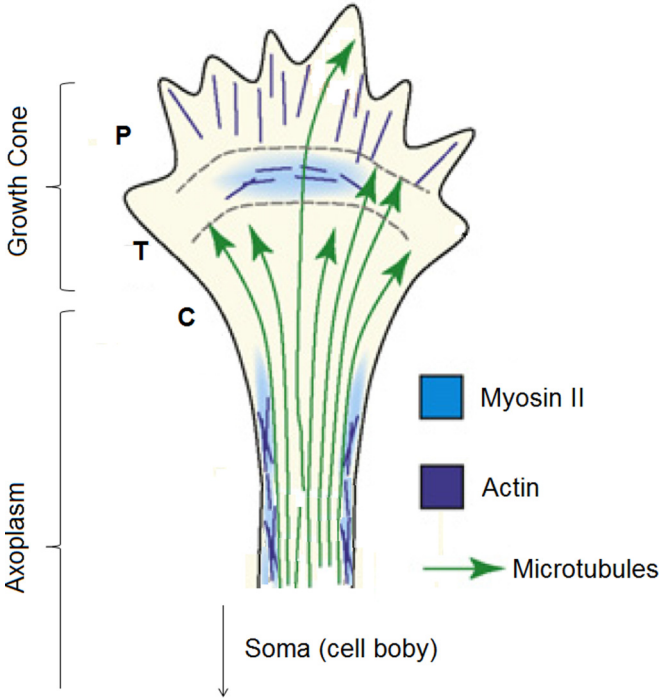


FIG. 1. Schematic representation of the cytoskeleton of a neurite extending from the soma. Adapted from Ref. [24].

rate of polymerization of microtubules depends on the force applied at their tip [37], both effects have been considered in a single simple model [38]. Experimentally, the physical forces arising from the F-actin or the microtubule meshworks are important since drug treatments that lower myosin II contractility (blebbistatin), prevent actin polymerization (cytochalasin B), depolymerize microtubules (nocodazole), or on the contrary stabilize them (taxol), each influence the tip velocity of a crawling neurite in a concentration-dependent manner [15,24,39–42]. Interestingly, different levels of cytochalasin B can lead to either an increase [40] (high level) or a decrease [43] (low level) in speed. This dependence suggests an antagonistic role of the acto-myosin meshwork in the propulsion.

Mechanical models require a rheological characterization of the axoplasm and the GC. The axoplasm has been described as a Burgers viscoelastic material based on its fast elastic response (seconds to minutes) to a force applied laterally or at the tip [44–46] while it elongates at a constant rate on longer time scales (a few hours) in response to a constant high force [32,33]. In Refs. [32,33], experiments tracking the mitochondria docked on the microtubule array have shown that, close to the T-domain, this network flows forward with a velocity comparable to the velocity of the neurite. Away from the T-domain toward the soma, the velocity decays exponentially, suggesting a fluidlike behavior of the neurite. However, if the applied force is not large enough, the neurite may undergo a finite deformation instead of acquiring a finite velocity [47], and both rheological models of Refs. [44] and [46] indicate a long-term stiffness of the neurite two orders of magnitude smaller than the short-time one. Furthermore, the loading rate is also known to play an important role in

the possible action potential impairment of the axon or in the transport properties alteration resulting from a loss of connectivity of the microtubule network [18,48–50]. Dynamic loading is not studied in this article, and the loading is assumed to be quasistatic. Axoplasm active growth and contractility have been proposed as the potential drivers for retraction or elongation of the neurite in the presence of an applied force [44], and contractility is explicitly incorporated as a force opposing elongation in Refs. [33,46].

The GC has been characterized as a Maxwell viscoelastic fluid with a relaxation time of a few seconds and an active contractile prestress stemming from the motor activity at the rear of the cone [51]. The F-actin polymerization-driven formation of filopodia extension and retraction has been physically described in Refs. [52,53].

In the present paper, we follow the suggestion of Ref. [33] that the theory of active gel may be used to unify these aforementioned models in order to obtain a global picture of neurite motility. Our one-dimensional model is based on the particular geometry of the neurite cytoskeleton and fundamental balance laws. An analysis of its solutions reveals that, depending on the neurite passive and active rheology, the neurite can collapse to the soma, remain static, or grow at finite velocity. The interchangeability of these three states is consistent with experiments that modify the state of the cytoskeleton and its substrate adhesivity with drugs.

In particular, we recover within a common framework the following general trends emerging from different sets of experiments probing the mechanical and structural environment of growing neurites:

(i) *Growth under axial force.* As mentioned above and already observed 30 years ago [30], a steady axial force applied by a cantilever at the proximal tip of a neurite elongates it [31–33,44,47,54,55]. This elongation is elastic if the force is below a certain threshold. Above that threshold, the neurite grows with finite velocity [56].

(ii) *Retraction under microtubules depletion.* As shown in Ref. [57], neurites retract in response to microtubule depletion and elongate even *in vivo* following stimulation of microtubules polymerization [58].

(iii) *Retraction with reduction of adhesivity.* By culturing neurites on different substrates, it was shown that retraction is promoted when the substrate adhesivity is reduced [33].

(iv) *Velocity increases with compliance.* Another important set of experiments shows that unlike other well-studied types of cells specialized in motion such as keratocytes or fibroblasts, neurites tend to go faster on compliant substrates than on stiff ones [23,59,60].

(v) *Motility is related to contractility.* Finally, neurites initiate their motility in a robust way when exposed to drugs that impair their active contractility [42,61].

The last two effects [62] are particularly important as possible therapeutic targets to promote axon regeneration after trauma [61].

The paper is organized as follows: In Sec. II, we develop a mechanical model for the axoplasm (acto-myosin and microtubule phases) alone and study its motility properties under an applied proximal traction force. In Sec. III, we model the GC (acto-myosin phase only) motile properties in response to a traction force applied at the trailing edge. In Sec. IV, we

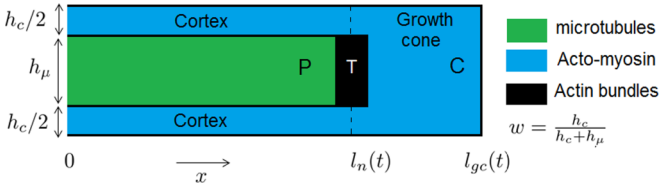


FIG. 2. Schematic of the neurite model geometry.

combine both models by assuming stress continuity at the T-domain to obtain a complete model of a growing neurite, and we show that it compares well with experiments.

II. AXOPLASM PROPULSION

Following Ref. [63], we model the microtubule network core of the axoplasm as a one-dimensional morphoelastic rod whose material points are indexed by the coordinate $x \in [0, l_n(t)]$, 0 denoting the connection with the soma and $l_n(t)$ the moving boundary between the GC and the axoplasm (T-domain), as shown in Fig. 2. Notice that our model does not separate the contribution of the neurofilaments from that of the microtubules. They are thus viewed as a passive reinforcing structure contributing to the overall network elasticity [14]. This rod can only deform along the axis and is in frictional contact with a viscous contractile “sleeve” (the cortex) that is supported by a static background. The tip of the neurite is subjected to a given traction force exerted either by the GC in normal growth conditions or by a micropipette, in experiments where the GC is lifted from the substrate [33].

A. Balance of mass

1. Microtubule network

Let ρ_μ denote the mass density of microtubules and v_μ their velocity in the laboratory reference frame. The mass balance equation reads

$$\partial_t \rho_\mu + \partial_x (\rho_\mu v_\mu) = S_\mu, \quad (1)$$

where the source term

$$S_\mu = k_p^\mu - k_d^\mu \rho_\mu \quad (2)$$

follows a first-order kinetic with a polymerization rate k_p^μ and a depolymerization term $k_d^\mu \rho_\mu$, proportional to the density [64]. We assume here that the tubulin (microtubule subunits) concentration is homogeneous [65] along the neurite because its motor-driven transport from distributed storage reservoirs along the axon is much faster ($\sim 1 \mu\text{m s}^{-1}$) than the crawling velocity ($\sim 10 \mu\text{m h}^{-1}$). We can rewrite Eq. (2) as $S_\mu = (\bar{\rho} - \rho_\mu)/\tau$, where $\bar{\rho} = k_p^\mu/k_d^\mu$ is the density at chemical equilibrium and $\tau = 1/k_d^\mu$ is the turnover time scale associated with microtubule renewal. Here we have adopted a mean-field description of the network, and we do not consider the microtubule polarity. Indeed, while this information is likely to be important for transport properties along the neurite, microtubules have a clear forward polarity in the axon and a mixed one in dendrites [8]. Yet, these two structures can move equivalently, suggesting that polarity may not be a fundamental variable in this physical process. Also note that while we do not account for the influence

of a potential loading on the kinetic rates k_p^μ and k_d^μ , our mean-field description captures the load-dependent dynamic of the whole microtubule array (see Sec. II E).

Assuming that no microtubule comes from the growth cone, Eq. (1) is equipped with a no-flux boundary condition at the tip of the neurite,

$$\dot{l}_n = v_\mu(l_n(t), t). \quad (3)$$

For simplicity, we also impose a no-flux boundary condition at the connection with the soma, so that $v_\mu(0, t) = 0$. Notice that at both ends, there is no assumption on the flux of tubulin, which adjusts to maintain a constant concentration as hypothesized in (2).

2. Cortical network

Denoting by ρ_c the mass density of actin in the cortex, we can write a conservation equation similar to Eq. (1):

$$\partial_t \rho_c + \partial_x (\rho_c v_c) = S_c, \quad (4)$$

where v_c is the velocity of the actin network in the cortex in the laboratory reference frame. However, we assume that the actin network is highly compressible compared to the microtubule network. Therefore, this equation decouples from the rest of the system, and the actin density can be found post-factum when the velocity field v_c is known using the method of characteristics [66]. This point is not tackled in the present paper, and S_c is thus left unspecified.

We again assume that there is no filamentous actin flux from the soma to the cortex: $v_c(0, t) = 0$. Unlike the microtubule network, the cortical actin is not stopped at the T-domain and can flow freely in the growth cone. Thus, there is no condition such as Eq. (3) for the cortical flow.

B. Balance of linear momentum

1. Microtubule network

The microtubule network is in contact with the cortical actin network through different types of cross-linking proteins that can actively bind and unbind (see Ref. [8] for a review). Assuming a sufficiently fast binding or unbinding dynamic [67], we model this contact as a viscous friction. Neglecting inertia, the balance of linear momentum reads

$$\partial_x \sigma_\mu = \zeta_\mu (v_\mu - v_c), \quad (5)$$

where ζ_μ is a friction coefficient and σ_μ is the internal axial stress rescaled by the microtubule network width, that is, if h_c is the width of the cortex and h_μ is the width of the microtubule network, both assumed to be constant, then $\sigma_\mu = (1 - w)\Sigma_\mu$, where Σ_μ is the axial Cauchy stress (axial force per unit area). We denote

$$w = \frac{h_c}{h_\mu + h_c} \in [0, 1]$$

as the ratio of the cortical over the total width of the axon.

At the leading edge, the axoplasm is subjected to a traction stress Q . Thus, the boundary condition associated with Eq. (5) reads

$$\sigma_\mu(l_n(t), t) = (1 - w)Q.$$

2. Cortical network

Similarly, the linear momentum balance in the cortical layer reads

$$\partial_x \sigma_c = -\zeta_\mu (v_\mu - v_c) + \zeta_c v_c, \quad (6)$$

where ζ_c is a friction coefficient of the cortex with respect to the substrate through adhesive proteins [22]. Here, $\sigma_c = w \Sigma_c$ is the rescaled axial stress, so that the boundary condition at the leading edge is

$$\sigma_c(l_n(t), t) = wQ.$$

C. Constitutive relations

To close our system of equations, we posit two assumptions about the rheology of the microtubules and cortical networks.

1. Microtubule network

Given the long turnover time of microtubules inside the axoplasm (which are highly stabilized [5,8]) and their high stiffness compared to F-actin filaments, we consider this network to be elastic for the time scale of interest (hours). We assume a logarithmic elastic stress-strain dependence

$$\sigma_\mu = -(1-w)E \log\left(\frac{\rho_\mu}{\rho_0}\right), \quad (7)$$

which has the advantage of preventing both infinite contraction and dilation. The natural density of microtubules at which no stress is created is ρ_0 . In principle, this density can be modulated by the presence of molecular motors in the microtubule array [33]. It is worth mentioning that our results are robust with respect to the choice of increasing concave functions other than log. In fact, realistic parameters show that ρ_μ is rather close to ρ_0 , thus implying that in the range of strain considered in physiological conditions, a linear relation between the stress and the local density (representing the strain in one dimension) could potentially be acceptable as well.

2. Cortical network

The turnover duration of an actin fiber in the cortex is fast (a few seconds [8,51]), and we use a linear viscous law for this phase to relate the stress to the strain rate. In addition, we assume that there is an active contractile stress created by the myosin II motor activity [19]:

$$\sigma_c = w(\eta \partial_x v_c + \chi c). \quad (8)$$

The bulk viscosity of F-actin is η , $\chi > 0$ is the contractility coefficient, and c is the concentration of motors. The conservation equation for c is (see Refs. [68,69] for further details)

$$\partial_t c + \partial_x (c v_c) - D \partial_{xx} c = \frac{\bar{c} - c}{\tau_c}. \quad (9)$$

The motors are advected with the actin filament that they bind but can also thermally diffuse with a diffusion coefficient D . The linear reaction term accounts for the attachment or detachment of motors with a cycle time τ_c . The concentration of motors at chemical equilibrium is \bar{c} . We can supplement this equation with a no-flux boundary condition at the soma,

$\partial_x c(0, t) = 0$, and assume that the motor concentration in the T-domain is a constant, $c(l_n(t), t) = c_0$.

Note that we do not resolve the radial component of the stress in our model (similarly to a neurite constrained in a channel [70]). Radial stress will be important for further investigation on the shape and turning of neurites, which is beyond the scope of this paper.

D. Final system

Denoting by $\sigma = \sigma_c + \sigma_\mu$ the total stress, $v = v_c$ the velocity of actin, and $\rho = \rho_\mu$ the density of microtubules, combining our model equations, we obtain the final system,

$$\begin{aligned} -\frac{w\eta}{\zeta_c} \partial_{xx} \sigma + \sigma &= w\chi c - E(1-w) \log\left(\frac{\rho}{\rho_0}\right), \\ \partial_t \rho + \partial_x (\rho v) - \frac{E(1-w)}{\zeta_\mu} \partial_{xx} \rho &= \frac{\bar{\rho} - \rho}{\tau}, \\ \partial_t c + \partial_x (c v) - D \partial_{xx} c &= \frac{\bar{c} - c}{\tau_c}, \end{aligned} \quad (10)$$

where the velocity field is related to the stress by $v = \partial_x \sigma / \zeta_c$. The boundary conditions are

$$\begin{aligned} \partial_x \sigma|_0 &= 0, \quad \partial_x \rho|_0 = 0, \quad \text{and} \quad \partial_x c|_0 = 0, \\ \sigma|_{l_n} &= Q, \quad \rho|_{l_n} = \rho_0 e^{-Q/E}, \quad \text{and} \quad c|_{l_n} = c_0. \end{aligned} \quad (11)$$

The last no-flux boundary condition,

$$\dot{l}_n = v|_{l_n} - \frac{E(1-w)}{\zeta_\mu} \frac{\partial_x \rho}{\rho} \Big|_{l_n(t)}, \quad (12)$$

is a Stefan condition needed to compute the unknown time dependence of the free boundary $l_n(t)$. In general, initial conditions should also be given, but here we focus on steady states only. The second equation in Eqs. (16) is obtained by expressing the velocity v_μ using Eq. (5) and combining it with Eq. (1).

We comment on the structure of Eqs. (10): the stress is created nonlocally over the so-called hydrodynamic length $l_c = \sqrt{\eta/\zeta_c}$ by two active agents. Motors from the cortex are pullers creating a contractile stress, and microtubules, provided their density is larger than ρ_0 , are pushers creating a tensile stress due to the addition of tubulin subunits in the network (growth). If tubulin subunits are removed (shrinking), the microtubules are also pullers. In the context of cell motility, such structures with pushers and pullers have been investigated in Refs. [71,72], where it was shown that growing and contracting agents can conspire to achieve robust motile properties of an active segment. Here, we supplement the picture with the two simple and similar dynamic equations in Eqs. (10) (second and third equations in that group) ruling the distribution of pushers and pullers that are relevant in the case of axonal motility.

Having already investigated the pullers-dominated case in Ref. [73] for motility properties and for the formation of periodic F-actin rings [69], which are actually observed in axons [8,74], we turn our attention to the pushers-dominated case. To understand this regime, from hereon we restrict our attention to the case in which the concentration of motors is homogeneous in the cortex, i.e., $c \equiv \bar{c}$. The resulting system

can then be rewritten in the following minimal form:

$$w\eta\partial_{xx}v - \zeta_c v = E(1-w)\frac{\partial_x\rho}{\rho}, \quad (13)$$

$$\partial_t\rho + \partial_x(\rho v) - \frac{E(1-w)}{\zeta_\mu}\partial_{xx}\rho = \frac{\bar{\rho} - \rho}{\tau},$$

with boundary conditions

$$v|_0 = 0 \quad \text{and} \quad \partial_x\rho|_0 = 0, \quad (14)$$

$$\eta\partial_x v|_{l_n} = Q - \chi\bar{c} \quad \text{and} \quad \rho|_{l_n} = \rho_0 e^{-Q/E},$$

along with the Stefan condition in Eq. (12). Substituting the nondimensional quantities,

$$\tilde{\sigma} = \frac{\sigma}{E}, \quad \tilde{x} = \frac{x}{\sqrt{\eta/\zeta_\mu}}, \quad \tilde{t} = \frac{t}{\eta/E}, \quad (15)$$

$$\tilde{\rho} = \frac{\rho}{\bar{\rho}}, \quad \text{and} \quad \tilde{Q} = Q/E,$$

in Eqs. (13) and (14) and dropping the tildes for clarity, we obtain the system

$$w\partial_{xx}v - av = (1-w)\frac{\partial_x\rho}{\rho}, \quad (16)$$

$$\partial_t\rho + \partial_x(\rho v) - (1-w)\partial_{xx}\rho = \epsilon(1-\rho),$$

with boundary conditions

$$v|_0 = 0 \quad \text{and} \quad \partial_x\rho|_0 = 0, \quad (17)$$

$$\partial_x v|_{l_n} = Q - Q_c \quad \text{and} \quad \rho|_{l_n} = e^{Q_\mu - Q},$$

and the free boundary condition,

$$\dot{l}_n = v\Big|_{l_n} - (1-w)\frac{\partial_x\rho}{\rho}\Big|_{l_n(t)}. \quad (18)$$

We have now six nondimensional parameters:

- (i) w , the relative width of the cortex with respect to the microtubule network.
- (ii) $a = \zeta_c/\zeta_\mu$, the ratio of friction coefficients.
- (iii) $\epsilon = \eta/(\tau E)$, the ratio of the acto-myosin over microtubule network viscosities.
- (iv) Q , the applied load at l_n scaled by E .
- (v) $Q_c = \chi\bar{c}/E > 0$, the scaled contractile load.
- (vi) $Q_\mu = -\log(\bar{\rho}/\rho_0)$ (see below).

Note that these six nondimensional parameters could be reduced to five by defining $\hat{Q} = Q - Q_\mu$ and $\Delta Q_\mu^c = Q_c - Q_\mu$. However, to keep the treatment of the microtubule and acto-myosin meshwork parallel, we keep the three distinct loads.

The system of Eqs. (16)–(18) cannot be explicitly solved, but some asymptotic cases provide insight into how the physics of such a medium works.

E. “Solid” and “fluid” asymptotic cases

1. The no-microtubule case, $w \rightarrow 1$

In the absence of microtubules, the velocity field can be solved directly from the first equation in Eqs. (18) and we obtain

$$v(x,t) = \frac{Q - Q_c}{\sqrt{a}} \frac{\sinh(\sqrt{a}x)}{\cosh[\sqrt{a}l_n(t)]}.$$

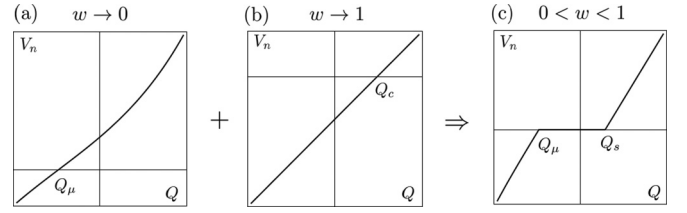


FIG. 3. (a) Velocity-force relation in the absence of a cortical acto-myosin network. (b) Velocity-force relation in the absence of a microtubule network. (c) Two thresholds velocity force in the general case.

Plugging this expression into Eq. (18) leads to

$$\dot{l}_n(t) = \frac{Q - Q_c}{\sqrt{a}} \tanh[\sqrt{a}l_n(t)].$$

This case was investigated in the absence of contraction ($Q_c = 0$) in Ref. [32] and successfully compared to experiments in which the GC was lifted and the axon was mechanically pulled with a cantilever. Notice, however, that in Ref. [32] v is the microtubule velocity, while here v is the velocity of F-actin.

The importance of axoplasmic contraction ($Q_c \neq 0$) was recently demonstrated in Ref. [33]. In this case, there are two possible steady states. Either the loading is larger than the contractile stress, $Q \geq Q_c$, and the axon then extends at the finite velocity $V_n = \dot{l}_n = (Q - Q_c)/\sqrt{a}$, or the loading is weaker than the contractile stress, $Q < Q_c$, and the neurite then collapses back to the soma. We sketch the force velocity $V_n(Q)$ relation in Fig. 3 (middle panel). This case can be referred to as “fluidlike” growth given that the axoplasm is effectively modeled as a contractile viscous fluid. Alternatively, it was shown in Ref. [75] that this case can also be described as a morphoelastic rod by combining an elastic response with a fast evolution of the reference configuration.

2. The no-cortex case, $w \rightarrow 0$

In the absence of a cortex, we combine Eqs. (16) to obtain the linear equation

$$\partial_t\rho - (1 + a^{-1})\partial_{xx}\rho = \epsilon(1 - \rho).$$

Its long-time asymptotics, on a semi-infinite domain $x \leq l_n(t)$, can be found by considering the traveling-wave reduction $y = x - l_n(t)$ in the domain $y < 0$, with $l_n(t) = V_n t$. Denoting by (\cdot) the derivative with respect to y , we obtain

$$-V_n\rho - (1 + a^{-1})\rho'' = \epsilon(1 - \rho),$$

with boundary conditions

$$\rho|_0 = e^{Q - Q_\mu}, \quad \partial_x\rho|_{-\infty} = 0,$$

and the front velocity given by

$$V_n = -(1 + a^{-1})e^{Q_\mu - Q}\partial_x\rho|_0.$$

The solution of this linear problem is given by

$$\rho(y) = 1 - \frac{p(Q)}{1 + p(Q)} e^{y/l(Q)}.$$

This expression depends on $l(Q)$, which can be interpreted as the typical size of a boundary layer, over which the

chemical reaction of polymerization or depolymerization of microtubules is maintained out of equilibrium at the tip of the neurite:

$$l(Q) = \sqrt{\frac{(1+a^{-1})[1+p(Q)]}{\epsilon}}.$$

The parameter $p(Q) = e^{Q-Q_\mu} - 1 > -1$ represents the driving force leading to expansion or retraction. Indeed, the tip velocity can be expressed as

$$V_n = \frac{p\sqrt{\epsilon(1+a^{-1})}}{\sqrt{1+p}}.$$

If $p < 0$ ($Q < Q_\mu$), then the combined effect of external force and shrinking of microtubules leads to a collapse back to the soma, while if $p > 0$ ($Q > Q_\mu$) the stress provided from microtubule growth is large enough to overcome an external load, and a steady expansion is predicted. In the absence of molecular motors, that is, without contraction, $Q_\mu < 0$ as microtubules are able to push [37]. However, in the presence of molecular motors, the sign of Q_μ cannot be readily established [33]. We sketched the force velocity $V_n(Q)$ relation in Fig. 3 (left panel). In this case, the neurite is effectively modeled as a growing elastic solid.

Notice that the velocity of the microtubules,

$$v_\mu = (1+a^{-1})\frac{\partial_y \rho}{\rho} = \frac{p(1+a^{-1})e^{y/l}}{l(1+p-pe^{y/l})},$$

also displays an exponential decay away from the tip of the neurite. This behavior is consistent with the experiments of Ref. [32].

From the two limiting cases discussed above, we can obtain a general picture of the dynamics when $0 < w < 1$ for small and large values of the applied load Q :

(i) If $Q < Q_\mu$, the axoplasm will collapse back to the soma. Indeed, both the cortex and the microtubule networks are in a collapse mode.

(ii) If $Q > Q_c$, the axon length will increase at a finite velocity given that both the cortex and the microtubule network are in extension.

Next, we consider the interval $Q \in [Q_\mu, Q_c]$ by studying possible static states in which a finite load does not lead to motion.

F. Static states

Static states are the solutions of the following problem:

$$\begin{aligned} w\partial_{xx}v - av &= (1-w)\frac{\partial_x \rho}{\rho}, \\ \partial_x[\rho v - (1-w)\partial_x \rho] &= \epsilon(1-\rho), \end{aligned} \quad (19)$$

with the boundary conditions of Eq. (17) and where l_n is a constant given by the condition

$$v|_{l_n} = (1-w)\frac{\partial_x \rho}{\rho}|_{l_n(t)}.$$

While there is no obvious solution to this nonlinear problem, the following two limiting cases shed light on the general case.

1. Large microtubule network viscosity, $\epsilon \rightarrow 0$

In the limit in which the microtubule network viscosity is much larger than the acto-myosin network viscosity, we can take the limit $\epsilon \rightarrow 0$. In this case, the second equation in Eqs. (19) can be solved exactly:

$$\rho(x) = \exp\left(Q_\mu - Q + \frac{\sigma(x) - Q}{a(1-w)}\right), \quad (20)$$

which can then be substituted into the first equation in Eqs. (19) to obtain

$$w\partial_{xx}v - (1+a)v = 0.$$

The solution of this last equation is simply

$$v(x) = (Q - Q_c)\sqrt{\frac{w}{1+a}} \frac{\sinh\left(\frac{x}{\sqrt{\frac{w}{1+a}}}\right)}{\cosh\left(\frac{l_n}{\sqrt{\frac{w}{1+a}}}\right)}.$$

The stress is obtained by integrating v :

$$\sigma(x) = \frac{wa}{1+a}(Q - Q_c) \frac{\cosh\left(\frac{l_n}{\sqrt{\frac{w}{1+a}}}\right) - \cosh\left(\frac{x}{\sqrt{\frac{w}{1+a}}}\right)}{\cosh\left(\frac{l_n}{\sqrt{\frac{w}{1+a}}}\right)},$$

which can be substituted back into Eq. (20) to obtain a closed expression for the density. The last constraint is provided by integrating the second equation in Eqs. (16) and requiring that for steady states the average density of microtubules is conserved, i.e.,

$$\frac{1}{l_n} \int_0^{l_n} \rho(x) dx = 1.$$

This constraint is now an integral equation for the static length l_n :

$$l_n e^{Q-Q_\mu} = \int_0^{l_n} \exp\left\{-f_0(Q - Q_c) \left[1 - \frac{\cosh\left(\frac{x}{\sqrt{\frac{w}{1+a}}}\right)}{\cosh\left(\frac{l_n}{\sqrt{\frac{w}{1+a}}}\right)}\right]\right\} dx, \quad (21)$$

where the constant f_0 reads $f_0 = w/[(1+a)(1-w)]$. In Appendix A, we show that there exists a steady solution for $Q \in [Q_\mu, Q_s^0]$ with

$$Q_s^0 = \frac{Q_\mu + f_0 Q_c}{1 + f_0}. \quad (22)$$

The parameter Q_s^0 is an average of Q_μ and Q_c weighted by the cortical width and the friction coefficients. The numerical solution of Eq. (21) between the two threshold loads is given in Fig. 4. The static length increases monotonically from 0 to ∞ between Q_μ and Q_s^0 .

2. Large cortex viscosity, $\epsilon \rightarrow \infty$

In this limit, it is clear from the right-hand side of the second equation in Eqs. (16) that ρ converges to 1 almost everywhere in the layer, except in a boundary layer close to the tip, where it has to satisfy the constraint $\rho|_{l_n} = e^{Q_\mu - Q}$. To obtain the dynamics of the moving front l_n , we use the piecewise linear

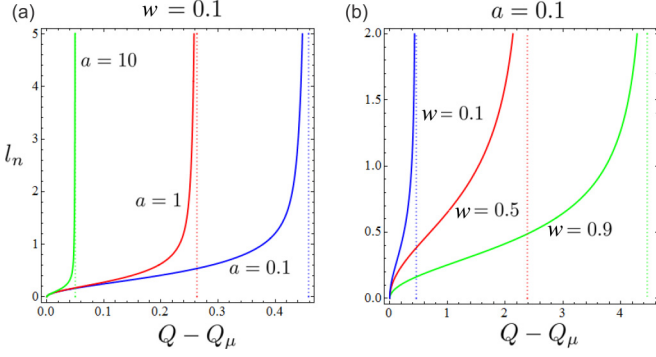


FIG. 4. Length-force relations for the static solutions given by Eq. (21) for different values of (a) a and (b) w . Parameter $\Delta Q_\mu^c = 5$.

ansatz:

$$\rho_\epsilon = \begin{cases} 1 & \text{if } x < l_n - \frac{1}{\epsilon}, \\ \epsilon(e^{Q_\mu - Q} - 1)\left(x + \frac{1}{\epsilon} - l_n\right) + 1 & \text{if } x > l_n - \frac{1}{\epsilon}. \end{cases}$$

Using this ansatz, we solve the first equation in Eqs. (16) to obtain $v(l_n)$ asymptotically in $1/\epsilon$. To leading order, we have

$$v(l_n) = \frac{(1-w)(1 - e^{Q_\mu - Q}) + w(Q - Q_c) \text{th}\left(\frac{\sqrt{a}l_n}{\sqrt{w}}\right)}{e^{Q_\mu - Q} \sqrt{wa}}.$$

This value is finite because the left-hand side of the first equation in Eqs. (16) is a regularizing elliptic operator. To leading order, the front dynamics is then given by

$$V = \dot{l}_n \sim (1-w)\sqrt{a}\epsilon \frac{1 - e^{Q_\mu - Q}}{e^{Q_\mu - Q}}.$$

We conclude that in the large- ϵ regime, there is no static front unless $Q = Q_\mu$. For $Q > Q_\mu$, the axon increases indefinitely and collapses for $Q < Q_\mu$.

G. General behavior

Rather than tackling the difficult questions of uniqueness and stability (both local and global) of the solutions that we have given in the previous sections, we use a numerical integration of problem (16) to build the phase diagram shown in Fig. 5 (see Appendix B for the method). For a given set of parameters w , a , and ΔQ_μ^c , we show in the (Q, ϵ) plane the domain of existence of the three observed behaviors: collapse, static, and motile.

Essentially, the overall behavior at finite ϵ is as follows:

(i) For $Q < Q_\mu$, we observe a collapse of the neurite back to the soma. This collapse is associated with a backward flow of microtubules along the entire axoplasm (see Fig. 5) as observed experimentally [33]. We find numerically that the time to collapse decreases with increasing ϵ since the effective resistance of the microtubule network to contraction decays.

(ii) For $Q_\mu \leq Q \leq Q_s$, where $Q_\mu < Q_s < Q_s^0$, we observe a stabilization of the neurite in a static state stemming from an interplay between the growing core and the surrounding contractile sleeve. Therefore, these static states may be interpreted as a tensile tightening of two parallel active networks.

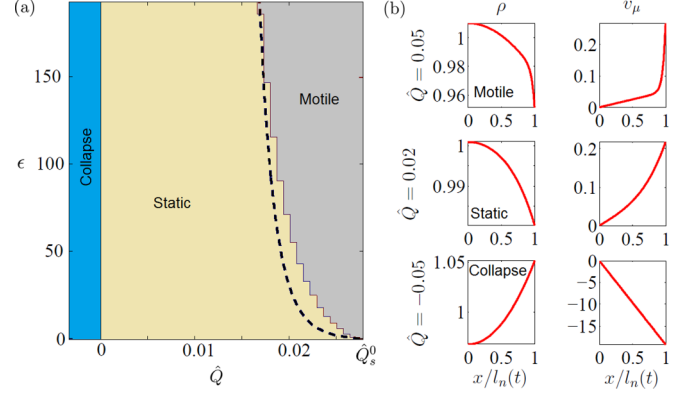


FIG. 5. (a) Numerically constructed phase diagram of the axoplasm. Parameters are $a = 0.1$, $w = 0.1$, and $\Delta Q_\mu^c = 0.3$. The dashed line is the analytic approximation from the metamodel presented in Sec. II G. (b) Typical steady-state profiles of the microtubule velocity and density in the three phases for $\epsilon = 0.001$. The numerical method is presented in Appendix B.

(iii) For $Q > Q_s$, we observe that the neurite tip moves with a finite velocity that increases with ϵ . The microtubule flow increases toward the tip and develops a boundary layer at the junction with the GC, as observed experimentally [32,33].

Accordingly, the general qualitative picture for the velocity-force relation is given in Fig. 3(c).

This double force thresholds system is in agreement with experiments [56]. Physically, our model reveals that the applied tip stress Q (positive when the neurite is pulled and negative if it pushes against an obstacle) must be larger than the stress created by the growing microtubule network Q_μ to avoid collapse, but it must also be larger than the effective stalling stress Q_s of the entire structure to lead to steady elongation. See Fig. 3(c). Between these thresholds, the neurite effectively behaves like a neutral solid in the sense that an increase of force leads to a global strain of the neurite, which acquires a new rest length. We further speculate that the oscillations in the loading at the T-domain coming from oscillating filopodia [52] can lead to the small-scale stop and go motion [22] experimentally observed during elongation.

H. Further simplifications

Analytical estimates can be obtained if we further simplify the model by using the fact that microtubule growths are localized at the tip of the axoplasm and provide an effective advection velocity of the free boundary [19,76,77].

We assume that the axoplasm is a mixture of the contractile acto-myosin network (with fraction w) and the microtubule network (with fraction $1-w$). In the nondimensional notations used previously, the mechanics of the contractile phase is then given by

$$\begin{aligned} \sigma_c &= \partial_x v_c + Q_c, \\ \partial_x \sigma_c &= \zeta_{\text{eff}} v_c, \\ \partial_x \sigma_c|_0 &= 0 \text{ and } \sigma_c|_{l_n} = Q. \end{aligned} \quad (23)$$

Similarly, the growing microtubule phase is given by

$$\begin{aligned}\sigma_\mu &= \eta_{\text{eff}} \partial_x v_\mu + Q_\mu, \\ \partial_x \sigma_\mu &= v_\mu, \\ \partial_x \sigma_\mu|_0 &= 0 \quad \text{and} \quad \sigma_\mu|_{l_n} = Q,\end{aligned}\quad (24)$$

where $\zeta_{\text{eff}} = (1+a)^n$ and $\eta_{\text{eff}} = (1+\epsilon)^{-m}$ with parameters $n > 0$ and $m > 0$ chosen below. The front dynamics is given by the no-flux boundary condition,

$$\dot{l}_n = w v_c|_{l_n} + (1-w) v_\mu|_{l_n}.$$

Solving Eqs. (23) and (24) and assuming that $\sqrt{\eta_{\text{eff}}}$ is small enough (localized tip growth assumption) compared to l_n , the moving front dynamics is given by

$$\dot{l}_n = w(Q - Q_c) \tanh(\sqrt{\zeta_{\text{eff}}} l_n) + (1-w) \frac{Q - Q_\mu}{\sqrt{\eta_{\text{eff}}}}, \quad (25)$$

which has a similar behavior to that of the full model:

(i) For $Q < Q_\mu$, $l_n \rightarrow 0$ and the neurite collapses to the soma.

(ii) For $Q_\mu < Q < Q_s$, we have $l_n \rightarrow l_n^s$ and the neurite reaches a finite length given by

$$l_n^s = \frac{1}{\sqrt{\zeta_{\text{eff}}}} \operatorname{arctanh}\left(\frac{Q - Q_\mu}{f_{\text{eff}}(Q_c - Q)}\right), \quad (26)$$

where $f_{\text{eff}} = w/(1-w)\sqrt{\eta_{\text{eff}}/\zeta_{\text{eff}}}$. The threshold load is given explicitly by

$$Q_s = \frac{Q_\mu + f_{\text{eff}} Q_c}{1 + f_{\text{eff}}}.$$

To recover the value $Q_s \rightarrow Q_s^0$ [see Eq. (22)] in the limit $\epsilon \rightarrow 0$, we choose $n = 2$. Then, we also have $Q_s \rightarrow Q_\mu$ in the limit $\epsilon \rightarrow \infty$. Finally, the parameter $m \sim 1/5$ is chosen heuristically to approximate the value of Q_s given by the general phase diagram (see Fig. 5).

(iii) For $Q > Q_s$, we have $l_n \rightarrow \infty$ and the neurite reaches a finite velocity V_n given by

$$V_n = \frac{(1-w)}{\sqrt{\eta_{\text{eff}}}} (1 + f_{\text{eff}})(Q - Q_s). \quad (27)$$

III. GROWTH CONE PROPULSION

Ahead of the axoplasm, we do not distinguish the lamellipodial and filopodial phases of the GC in the following one-dimensional (1D) model. The GC is continuous with the acto-myosin cortex, and we will therefore model it as a visco-contractile material. We use the index gc to denote variables related to the GC.

A. Balance of mass

The mass balance for actin reads

$$\partial_t \rho_{gc} + \partial_x (\rho_{gc} v_{gc}) = -k_d \rho_{gc},$$

where ρ_{gc} is the density of F-actin and v_{gc} is its velocity in the laboratory reference frame. Here, k_d is the bulk depolymerization rate [68]. This equation is supplemented with the kinetic boundary condition

$$\dot{l}_{gc} = v(l_{gc}(t), t) + v_p,$$

where v_p is the localized polymerization (G-actin to F-actin) velocity at the tip of the GC [19,52,76]. More generally, v_p may also depend on the microtubules extending into the filopodium [35] and on the external loading [19] at the proximal tip of the GC, but we will not consider this dependence. Therefore, we assume here a stress-free leading edge. As in the previous discussion, the high compressibility of F-actin leads to the decoupling of the actin density with the front dynamic.

B. Balance of momentum

In the viscous regimes, the balance of linear momentum reads

$$\partial_x \sigma_{gc} = \zeta_c v_{gc}, \quad (28)$$

where ζ_c is the friction coefficient with respect to the substrate. This equation is supplemented with stress boundary conditions,

$$\sigma_{gc}|_{l_n(t)} = Q \quad \text{and} \quad \sigma_{gc}|_{l_{gc}(t)} = 0, \quad (29)$$

where, as before, Q denotes the common traction force in the T-domain at the axoplasm/GC interface. The leading edge of the cone is assumed to be stress-free.

C. Constitutive relation

The constitutive relation includes both a viscous and a contractile term:

$$\sigma_{gc} = \eta \partial_x v_{gc} + \chi \bar{c} - p. \quad (30)$$

The pressure p is defined numerically as a constant Lagrange multiplier associated with the conservation of the one-dimensional volume of the GC,

$$l_{gc}(t) - l_n(t) = L. \quad (31)$$

This constraint follows from both osmotic effects [78,79] and the fact that few compressible microtubules are engaged into filopodia [80].

More general models taking into account global compressibility of the GC may be required to access variation of L when some rheological parameters such as the tip growth velocity or the contractility are affected by drug treatments [81]. However, our goal here is to describe the entire neurite, and we will not discuss these finer effects further.

D. Crawling velocity of the cone

Combining Eqs. (28) and (30), we obtain

$$-l_c^2 \partial_{xx} \sigma_{gc} + \sigma_{gc} = \chi \bar{c} - p. \quad (32)$$

Solving Eq. (32) with boundary conditions [see Eq. (29)] and satisfying the constraint of fixed length [see Eq. (31)], we obtain a closed expression for σ_{gc} and v_{gc} that we use to compute the fronts dynamic (see Refs. [73,77] for further details):

$$\dot{l}_{gc} = \dot{l}_n = V_{gc} = \frac{1}{2} \left(v_p - \frac{Q}{\sqrt{\eta \zeta_c} \tanh(L/(2l_c))} \right).$$

Introducing the dimensionless velocities $\tilde{V}_{gc} = V_{gc}/(E/\sqrt{\eta \zeta_u})$ and $\tilde{v}_p = v_p/(E/\sqrt{\eta \zeta_u})$, $\tilde{Q} = Q/E$, this

TABLE I. Estimates of material coefficients.

Name	Symbol	Typical value
F-actin viscosity	η	10^3 Pa s [51]
Elasticity of microtubules	E	200–400 Pa [44–46]
Microtubule viscosity	$E\tau$	$(1-5) \times 10^6$ Pa s [32,33]
Viscous friction coefficient	ζ_c	$10^{14}-10^{15}$ Pa m $^{-2}$ s [23,32]
Contractility	$\chi\bar{c}$	$10-10^2$ Pa [33,45,46,51]
F-actin polymerization velocity	v_p	2×10^{-8} m s $^{-1}$ [19,52]
GC length	L	$(1-2) \times 10^{-5}$ m [33,51]
Cortex to axon width	w	0.1 [74]
Friction cortex/microtubules	ζ_μ	$10\zeta_c$ (estimated)
Hydrodynamic length l_c	$\sqrt{\eta/\zeta_c}$	$\sim 1.5 \times 10^{-6}$ m
Characteristic length	$\sqrt{\eta/\zeta_\mu}$	$\sim 4.4 \times 10^{-7}$ m
Characteristic time	η/E	~ 3 s
Characteristic velocity	$E/\sqrt{\eta\zeta_\mu}$	$\sim 1.5 \times 10^{-7}$ m s $^{-1}$
Characteristic stress	E	~ 300 Pa

last expression becomes

$$\tilde{V}_{gc} = \frac{1}{2} \left(\tilde{v}_p - \frac{\tilde{Q}}{\sqrt{a} \tanh(L/(2l_c))} \right).$$

From simple physical parameter estimates (see Table I), we have $L \gg 2l_c$ so that $\tanh[L/(2l_c)] \sim 1$, and we obtain, after dropping the tildes,

$$V_{gc} = \frac{1}{2} \left(v_p - \frac{Q}{\sqrt{a}} \right). \quad (33)$$

The GC is propelled by the polymerization of the actin network at the leading edge, which pushes the membrane forward. However, the GC is also pulled by the traction force at the interface with the axoplasm. This traction force decreases the velocity of migration if $Q > 0$. The GC stops moving when Q reaches the stall force,

$$Q_{gc} = \sqrt{a}v_p.$$

IV. FULL NEURITE CRAWLING

A. Overall behavior

We can now combine the models for the motion of the GC and the axoplasm parts to obtain a full picture of the neurite dynamics. We use the analytic relations derived in Secs. II G and III as they capture the main effects. We can distinguish three cases depending on the acto-myosin of the GC Q_{gc} :

(i) If $Q_{gc} < Q_\mu$, then the axon collapses to the soma in finite time.

(ii) If $Q_\mu < Q_{gc} < Q_s$, then the axon has a finite static length. Using the approximation given by Eq. (26), we have

$$l^s = \frac{1}{\sqrt{\zeta_{\text{eff}}}} \text{arctanh} \left(\frac{Q_{gc} - Q_\mu}{f_{\text{eff}}(Q_c - Q_{gc})} \right). \quad (34)$$

(iii) If $Q_s < Q_{gc}$, the axon acquires a finite steady-state velocity. Using the approximation given by Eqs. (27) and (33), we obtain

$$V = \frac{Q_{gc} - Q_s}{2\sqrt{a} + \frac{(1-w)}{\sqrt{\eta_{\text{eff}}}}(1 + f_{\text{eff}})}. \quad (35)$$

We conclude that the main behavior of the system is captured by the relative magnitude of the three stall forces of the different neurite phases: the microtubule network (Q_μ), the entire axoplasm (Q_s), and the acto-myosin of the GC (Q_{gc}).

B. Parameter estimation

The three loads Q_μ , Q_s , and Q_{gc} depend on six non-dimensional parameters directly related to measurable material coefficients. Based on Table I, we have

$$a \sim 0.1, \quad \epsilon \sim 0.001, \quad w \sim 0.1, \quad v_p \sim 0.14, \quad \text{and} \quad Q_c \sim 0.3.$$

It is more difficult to assess the value of the microtubule network stall force Q_μ as the presence of molecular motors may induce contraction [33]. In Ref. [35], it is shown that the growth of microtubules engaging in filopodia can lead to a pushing stress of -90 Pa at the tip. However, in agreement with Ref. [33], we assume that the axonal microtubules exert a small pulling stress. Here, we choose 9 Pa by setting the neurite velocity to about $10 \mu\text{m h}^{-1}$, leading to

$$Q_\mu \sim 0.03.$$

C. Comparison with experiments

Now that our model has been validated against classical pulling experiments, it is interesting to see how its predictions compare with various pharmacological tests affecting the F-actin and microtubules meshworks.

The effects of some classical drug treatments on the model parameters are collected in Table II.

1. Retraction under microtubules depletion

Experiments have shown that the depolymerization of microtubules with nocodazole stops or even leads to the collapse of neurites depending on the concentration [40,57,81]. This treatment can be interpreted in our model as an increase of k_d^μ and thus an increase of Q_μ and is qualitatively captured in Fig. 6.

Physically, the depolymerization of microtubules lowers the resistance of this growing network to contractile acto-myosin stress. As we show in the inset of Fig. 6 and as experimentally confirmed in Ref. [57], nocodazole induced collapse can be counteracted by a latrunculin (which destroys the acto-myosin cortex) or BDM (which inhibits myosin II contractile activity), which effectively reduces Q_c .

Conversely, initiation of motility due to blebbistatin treatment (contractility inhibitor) is abolished if it is followed by a nocodazole treatment [42]. Additionally, an increase of microtubule polymerization using epothilone B points toward a very promising therapeutic route to promote *in vivo* axonal outgrowth after injury of the spinal cord through the inhibitory environment due to the tissue scar [58]. Treatment with a high concentration of taxol stabilizes microtubules and slows down elongation [82–84]. This can be interpreted in the model as a decrease of ϵ and is also correctly captured, as seen in Fig. 6. However, the effect of a low concentration of taxol does not block the microtubule dynamics completely [84] but primarily lowers Q_μ (by lowering k_d^μ), thus leading to an increase of axonal outgrowth [84,85].

TABLE II. Effects of classical drugs.

Drug	Effect	Parameters trend
blebbistatin	inhibit myosin II contractility	$Q_c \downarrow$
BDM	inhibit myosin II contractility	$Q_c \downarrow$
cytochalasin	inhibit actin polymerization	$v_p \downarrow$ ($Q_c \downarrow$ high concentration)
latrunculin	destroys the actin meshwork	$v_p \downarrow, Q_c \downarrow$
nocodazole	depolymerizes microtubules	$Q_\mu \uparrow$
epothilone B	polymerizes microtubules	$Q_\mu \downarrow$
taxol	stabilizes microtubules	$\epsilon \downarrow$ ($Q_\mu \downarrow$ low concentration)
trypsin	detaches the neurite	$a \downarrow$

2. Treatment of the acto-myosin meshwork

We now turn to the treatments affecting the acto-myosin meshwork (Fig. 7), which has two antagonistic roles [25,39]. On the one hand, it is pulling the axoplasm thanks to F-actin front polymerization (v_p), but the contractile acto-myosin cortex is also pulling the neurite backward. Remarkably, treatment with a low concentration of cytochalasin [43] reduces only the front F-actin protrusion (no filopodia) and can be interpreted as lowering v_p effectively reducing the neurite velocity. Larger concentrations, on the contrary, destroy the whole F-actin meshwork, which strongly impacts the cortical contractility (Q_c) and leads to an increase of neurite velocity as captured by the model [40]. More focused experiments inhibiting contractility with blebbistatin [42,61] confirm that contractility impairment robustly initiates neurite motility. Note again that cytochalasin (v_p decrease) abolishes this blebbistatin induced motility [42] as the model also predicts; see Fig. 7.

3. Treatment of the substrate to modify adhesions

Adhesion of the neurite with the substrate can also be strongly reduced with trypsin, which leads to a collapse or

a stall of the neurite [33]. Such treatment can be modeled by lowering a . In Fig. 8(a), we show that this effect is correctly captured by our model. It is also known that the motility-promoting effect of myosin II inhibition is adhesiveness-dependent [42]. While blebbistatin promotes motility on polylysine substrates, it lowers motility on less adherent laminin substrates [62]. We can speculate that this is due to myosin II being strongly involved in the creation of focal adhesions for laminin substrates [15,62]. As a result, in this case, a blebbistatin treatment also considerably lowers adhesion (a), thus potentially leading to arrest [see Fig. 8(a)]. Finally, we also show in Fig. 8(b) the effect of a cytochalasin treatment depending on the substrate adhesivity. While a low level of cytochalasin reduces the neurite velocity, we expect this effect to be attenuated on more adhesive substrates. At a constant adhesion bond density and toughness, the effect of decreasing the substrate elasticity is to increase the friction coefficient ξ_c (see Ref. [86]), leading to an increase of a in the nondimensional parameters, and in turn to an increase of neurite motility. Hence, in this sense, our model also captures the counter durotactic tendency of neurites to be faster on softer substrates [59,60].

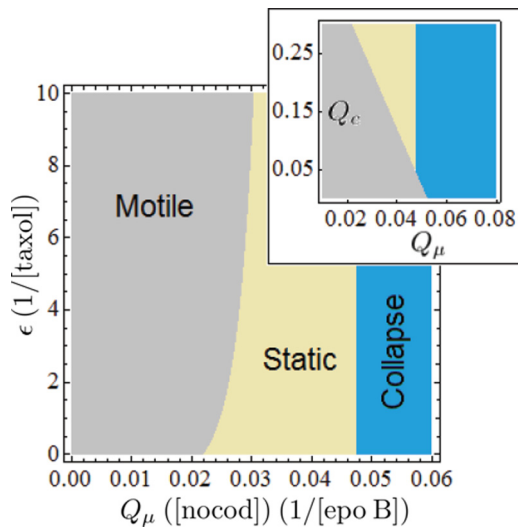


FIG. 6. Perturbation of the microtubule network properties by nocodazole and taxol (inset: latrunculin and BDM reducing Q_c): phase diagrams of the whole neurite state using expressions of the three driving loads Q_μ , Q_s , and Q_{gc} (default parameters are $a \sim 0.1$, $\epsilon \sim 0.001$, $w \sim 0.1$, $v_p \sim 0.14$, $Q_c \sim 0.3$, and $Q_\mu \sim 0.03$).

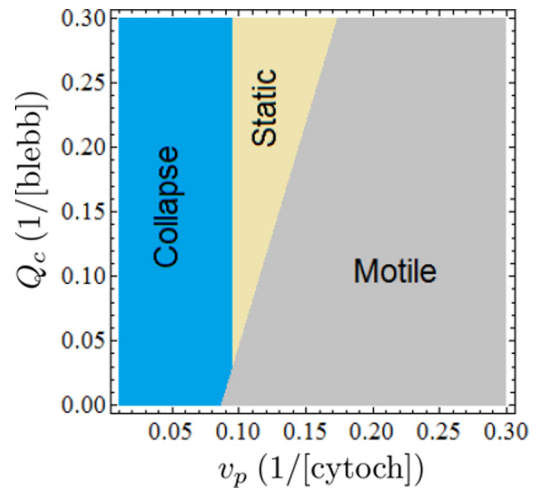


FIG. 7. Perturbations of the acto-myosin meshwork by cytochalasin and blebbistatin: phase diagram of the whole neurite state using expressions of the three driving loads Q_μ , Q_s , and Q_{gc} (default parameters are $a \sim 0.1$, $\epsilon \sim 0.001$, $w \sim 0.1$, $v_p \sim 0.14$, $Q_c \sim 0.3$, and $Q_\mu \sim 0.03$).

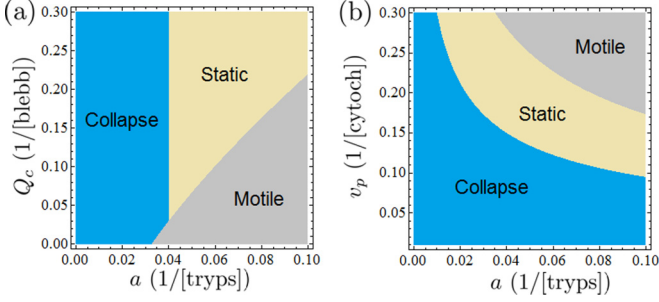


FIG. 8. Perturbations of the substrate adhesion by trypsin, blebbistatin, and cytochalasin: phase diagrams of the whole neurite state using expressions of the three driving loads Q_μ , Q_s , and Q_{gc} (default parameters are $a \sim 0.1$, $\epsilon \sim 0.001$, $w \sim 0.1$, $v_p \sim 0.14$, $Q_c \sim 0.3$, and $Q_\mu \sim 0.03$).

V. CONCLUSION

Starting from basic conservation laws, we have developed and analyzed a one-dimensional mechanical model of neurite motility based on a three-compartment cytoskeletal structure. The model supports three robust states: collapse, static, and motile. Collapse arises when the growth of the microtubules and the GC-induced traction cannot overcome the cortical actomyosin contractility. On the contrary, extension at a finite velocity is provoked by the GC F-actin frontal polymerization, which generates a tension promoting growth of the microtubule network and overcoming cortical contractility. Interestingly, between these two states, the neurite can also remain static as a result of a tensile tightening between the microtubule growing network and the contractile actomyosin sleeve operating in parallel.

The respective position of the three stall forces of the microtubules, the axoplasm, and the GC can be used to predict the state of the neurite, and we explicitly relate these loads to measurable material parameters. This framework allows for a number of model predictions in remarkable agreement with experimental drug treatments. It is our hope that the model will be used as a guideline to design focused experiments to discriminate the respective role of active (contractility, growth) and passive (elasticity, viscosity, substrate stiffness) effects impacting neurite motility and leading to a better understanding of the neuronal regeneration after a trauma.

We did not investigate the shape of neurites, which is also known to be an important signature of trauma [18,87] as neurons swell or bead in response to fast pulling. To deal with this complex problem, a two-dimensional model must be used and the osmotic pressure regulation between the inside and the outside of the neurite must be taken into account [87]. More generally, coupling of the cytoskeletal mechanics with the ions trafficking through channels and pumps at the plasmic membrane is an important challenge that will lead to better insight into neurite guidance by chemical gradients as well as the swelling of neurons during injury.

ACKNOWLEDGMENTS

P.R. acknowledges funding from OCCAM. P.R. and A.J. also acknowledge funding from the European Research

Council under the European Union's Seventh Framework Programme (FP7 2007-2013)/ERC Grant Agreement No. 306587.

APPENDIX A: EXISTENCE OF SOLUTIONS TO EQ. (21)

Equation (21) can be rewritten in the following form:

$$e^{\hat{Q}} = \psi(l_n), \quad \text{where } \psi(l_n) = \int_0^1 e^{[(1+f_0)Q_s^0 - f_0\hat{Q}]g(u,l_n)} du,$$

with

$$g(u,l_n) = 1 - \frac{\cosh\left(\frac{ul_n}{l_w}\right)}{\cosh\left(\frac{l_n}{l_w}\right)}$$

and $l_w = \sqrt{\frac{wa}{1+a}}$. Using the dominated convergence theorem, it follows that

$$\psi(0) = 1 \text{ and } \psi(\infty) = e^{[(1+f_0)Q_s^0 - f_0\hat{Q}]}$$

We also have

$$\begin{aligned} \frac{d\psi}{dl_n} &= \frac{(1+f_0)Q_s^0 - f_0\hat{Q}}{l_w \cosh\left(\frac{l_n}{l_w}\right)^2} \int_0^1 du e^{[(1+f_0)Q_s^0 - f_0\hat{Q}]g(u,l_n)} \\ &\quad \times \left[\cosh\left(\frac{ul_n}{l_w}\right) \sinh\left(\frac{l_n}{l_w}\right) - u \cosh\left(\frac{l_n}{l_w}\right) \sinh\left(\frac{ul_n}{l_w}\right) \right]. \end{aligned}$$

$\geq \sinh\left(\frac{l_n(1-u)}{l_w}\right) \geq 0$

As a result, if $\hat{Q} < Q_s$, then $\psi(l_n)$ is an increasing function. If we additionally have $\hat{Q} > 0$, then $e^{\hat{Q}}$ is strictly between $\psi(0)$ and $\psi(\infty)$ leading to the existence of a single solution of Eq. (21).

APPENDIX B: NUMERICAL METHOD

To solve the Cauchy problem of Eqs. (16) and (17), we use the scaled space coordinate to deal with the moving boundary,

$$y = \frac{x}{l_n(t)}, \quad (\text{B1})$$

and we denote the new unknown functions $\hat{v}(y,t) = v[l_n(t)y,t]$ and $\hat{\rho}(y,t) = l_n(t)\rho[l_n(t)y,t]$. The second equation in Eqs. (16) becomes

$$\partial_t \hat{\rho} + \frac{1}{l_n} \partial_y \left(\hat{\rho}(\hat{v} - y\dot{l}_n) - \frac{1-w}{l_n} \partial_y \hat{\rho} \right) = l_n \epsilon \left(1 - \frac{\hat{\rho}}{l_n} \right), \quad (\text{B2})$$

where the velocity field can be expressed through the first equation in Eqs. (16) as

$$\frac{w}{l_n^2} \partial_{yy} \hat{v} - a \hat{v} = \frac{1-w}{l_n} \frac{\partial_y \hat{\rho}}{\hat{\rho}}. \quad (\text{B3})$$

Accordingly, the boundary conditions of Eq. (17) become

$$\hat{v}|_0 = 0 \quad \text{and} \quad \partial_y \hat{v}|_1 = l_n(Q - Q_c), \quad (\text{B4})$$

$$\partial_y \hat{\rho}|_0 = 0 \quad \text{and} \quad \hat{\rho}|_1 = l_n e^{Q_\mu - Q}, \quad (\text{B5})$$

$$\dot{l}_n = \hat{v} \Big|_1 - \frac{(1-w)\partial_y \hat{\rho}}{l_n \hat{\rho}} \Big|_1. \quad (\text{B6})$$

To fully specify the system, we impose the initial conditions

$$l_n(0) = l_n^0 \quad \text{and} \quad \hat{\rho}(y, 0) = \hat{\rho}^0(y).$$

Numerically, we did not find that the steady-state phase reported in Fig. 5 was sensitive to the choice of initial conditions.

The numerical scheme used to solve the Cauchy problem, Eqs. (B2)–(B6), is based on the finite volume method [88], which allows to conserve mass while handling localized states without spurious oscillations. Two regularly spaced grids on the same interval $[0, 1]$, denoted Z and Z_d for its dual, are

considered in parallel. An initial condition on $\hat{\rho}$ being given on Z , Eq. (B3) is solved using the boundary conditions of Eq. (B4), and the effective drift term $\hat{v} - y\dot{l}_n$ is computed on Z_d using Eq. (B3). We then apply an upwind finite volume scheme to Eq. (B2) using the no-flux boundary conditions of Eq. (B5). This allows the computation of the updated concentration profile $\hat{\rho}$ on Z , which gives in turn the new initial data used for the next time step and the front dynamic through Eq. (B6). The same procedure is then repeated. The time interval for each time step is adapted so that the Courant-Friedrichs-Lewy condition is uniformly satisfied on Z_d [88].

-
- [1] S. R. Cajal and S. Cajal, *Histologie du Système Nerveux de l'Homme et des Vertébrés Maloigne* (Maloigne, Paris, 1911).
 - [2] J. Silver and J. H. Miller, *Nat. Rev. Neurosci.* **5**, 146 (2004).
 - [3] L. C. Case and M. Tessier-Lavigne, *Curr. Biol.* **15**, R749 (2005).
 - [4] R. Deumens, A. Bozkurt, M. F. Meek, M. A. Marcus, E. A. Joosten, J. Weis, and G. A. Brook, *Progr. Neurobiol.* **92**, 245 (2010).
 - [5] T. Mitchison and M. Kirschner, *Neuron* **1**, 761 (1988).
 - [6] E. W. Dent and F. B. Gertler, *Neuron* **40**, 209 (2003).
 - [7] K. Franze and J. Guck, *Rep. Prog. Phys.* **73**, 094601 (2010).
 - [8] C. H. Coles and F. Bradke, *Curr. Biol.* **25**, R677 (2015).
 - [9] M. Aeschlimann and L. Tettoni, *Neurocomputing* **38**, 87 (2001).
 - [10] B. J. Dickson, *Science* **298**, 1959 (2002).
 - [11] L. A. Lowery and D. Van Vactor, *Nat. Rev. Mol. Cell Biol.* **10**, 332 (2009).
 - [12] J. Reingruber and D. Holcman, in *Seminars in Cell & Developmental Biology* (Elsevier, Amsterdam, 2014), Vol. 35, pp. 189–202.
 - [13] K. Franze, J. Gerdemann, M. Weick, T. Betz, S. Pawlizak, M. Lakadamyali, J. Bayer, K. Rillich, M. Göglér, Y.-B. Lu *et al.*, *Biophys. J.* **97**, 1883 (2009).
 - [14] H. Ouyang, E. Nauman, and R. Shi, *J. Biol. Eng.* **7**, 21 (2013).
 - [15] J. Brown and P. C. Bridgman, *J. Histochem. Cytochem.* **51**, 421 (2003).
 - [16] D. H. Roossien, P. Lamoureux, and K. E. Miller, *J. Cell Sci.* **127**, 3593 (2014).
 - [17] W. Lu, P. Fox, M. Lakonishok, M. W. Davidson, and V. I. Gelfand, *Curr. Biol.* **23**, 1018 (2013).
 - [18] H. Ahmadzadeh, D. H. Smith, and V. B. Shenoy, *Biophys. J.* **106**, 1123 (2014).
 - [19] F. Julicher, K. Kruse, J. Prost, and J.-F. Joanny, *Phys. Rep.* **449**, 3 (2007).
 - [20] A. B. Verkhovskiy, T. M. Svitkina, and G. G. Borisy, *Curr. Biol.* **9**, 11 (1999).
 - [21] N. A. Medeiros, D. T. Burnette, and P. Forscher, *Nat. Cell Biol.* **8**, 216 (2006).
 - [22] L. Bard, C. Boscher, M. Lambert, R.-M. Mège, D. Choquet, and O. Thoumine, *J. Neurosci.* **28**, 5879 (2008).
 - [23] C. E. Chan and D. J. Odde, *Science* **322**, 1687 (2008).
 - [24] R. B. Vallee, G. E. Seale, and J.-W. Tsai, *Trends Cell Biol.* **19**, 347 (2009).
 - [25] M. Aeschlimann, Ph.D. thesis, Université de Lausanne, 2000.
 - [26] G. Kiddie, D. McLean, A. Van Ooyen, and B. Graham, *Prog. Brain Res.* **147**, 67 (2005).
 - [27] D. M. Suter and K. E. Miller, *Progr. Neurobiol.* **94**, 91 (2011).
 - [28] C. S. Peskin, G. M. Odell, and G. F. Oster, *Biophys. J.* **65**, 316 (1993).
 - [29] A. Mogilner and G. Oster, *Biophys. J.* **84**, 1591 (2003).
 - [30] D. Bray, *J. Cell Sci.* **37**, 391 (1979).
 - [31] P. Lamoureux, R. E. Buxbaum, and S. R. Heidemann, *Nature (London)* **340**, 159 (1989).
 - [32] M. O'Toole, P. Lamoureux, and K. E. Miller, *Biophys. J.* **94**, 2610 (2008).
 - [33] M. O'Toole, P. Lamoureux, and K. E. Miller, *Biophys. J.* **108**, 1027 (2015).
 - [34] M. P. Van Veen and J. Van Pelt, *Bull. Math. Biol.* **56**, 249 (1994).
 - [35] P. Rauch, P. Heine, B. Goettgens, and J. A. Käs, *New J. Phys.* **15**, 015007 (2013).
 - [36] J. García, J. Peña, S. Mchugh, and A. Jérusalem, *Comput. Model. Eng. Sci.* **87**, 411 (2012).
 - [37] M. Dogterom and B. Yurke, *Science* **278**, 856 (1997).
 - [38] R. Buxbaum and S. Heidemann, *J. Theor. Biol.* **155**, 409 (1992).
 - [39] P. C. Letourneau, T. A. Shattuck, and A. H. Ressler, *Cell Motil. Cytoskeleton* **8**, 193 (1987).
 - [40] T. Dennerll, H. Joshi, V. Steel, R. Buxbaum, and S. Heidemann, *J. Cell Biol.* **107**, 665 (1988).
 - [41] K. Kollins, J. Hu, P. Bridgman, Y.-Q. Huang, and G. Gallo, *Devel. Neurobiol.* **69**, 279 (2009).
 - [42] E.-M. Hur, I. H. Yang, D.-H. Kim, J. Byun, W.-L. Xu, P. R. Nicovich, R. Cheong, A. Levchenko, N. Thakor, F.-Q. Zhou *et al.*, *Proc. Natl. Acad. Sci. USA* **108**, 5057 (2011).
 - [43] J. Q. Zheng, J. Wan, and M. Poo, *J. Neurosci.* **16**, 1140 (1996).
 - [44] T. J. Dennerll, P. Lamoureux, R. E. Buxbaum, and S. R. Heidemann, *J. Cell Biol.* **109**, 3073 (1989).
 - [45] R. Bernal, P. A. Pullarkat, and F. Melo, *Phys. Rev. Lett.* **99**, 018301 (2007).
 - [46] R. Bernal, F. Melo, and P. A. Pullarkat, *Biophys. J.* **98**, 515 (2010).
 - [47] J. Zheng, P. Lamoureux, V. Santiago, T. Dennerll, R. E. Buxbaum, and S. R. Heidemann, *J. Neurosci.* **11**, 1117 (1991).
 - [48] A. Jérusalem, J. A. García-Grajales, A. Merchán-Pérez, and J. M. Peña, *Biomechan. Model. Mechanobiol.* **13**, 883 (2014).
 - [49] W. W. Ahmed and T. A. Saif, *Sci. Rep.* **4**, 4481 (2014).
 - [50] A. Shamloo, F. Manuchehrfar, and H. Rafii-Tabar, *J. Biomechan.* **48**, 1241 (2015).
 - [51] T. Betz, D. Koch, Y.-B. Lu, K. Franze, and J. A. Käs, *Proc. Natl. Acad. Sci. USA* **108**, 13420 (2011).
 - [52] T. Betz, D. Lim, and J. A. Käs, *Phys. Rev. Lett.* **96**, 098103 (2006).

- [53] E. M. Craig, D. Van Goor, P. Forscher, and A. Mogilner, *Biophys. J.* **102**, 1503 (2012).
- [54] P. Lamoureux, G. Ruthel, R. E. Buxbaum, and S. R. Heidemann, *J. Cell Biol.* **159**, 499 (2002).
- [55] T. D. Nguyen, I. B. Hogue, K. Cung, P. K. Purohit, and M. C. McAlpine, *Lab Chip* **13**, 3735 (2013).
- [56] S. R. Heidemann and R. E. Buxbaum, *Neurotoxicology* **15**, 95 (1993).
- [57] F. J. Ahmad, J. Hughey, T. Wittmann, A. Hyman, M. Greaser, and P. W. Baas, *Nat. Cell Biol.* **2**, 276 (2000).
- [58] J. Ruschel, F. Hellal, K. C. Flynn, S. Dupraz, D. A. Elliott, A. Tedeschi, M. Bates, C. Sliwinski, G. Brook, K. Dobrindt *et al.*, *Science* **348**, 347 (2015).
- [59] L. A. Flanagan, Y.-E. Ju, B. Marg, M. Osterfield, and P. A. Janmey, *Neurorep.* **13**, 2411 (2002).
- [60] P. C. Georges, W. J. Miller, D. F. Meaney, E. S. Sawyer, and P. A. Janmey, *Biophys. J.* **90**, 3012 (2006).
- [61] P. Yu, L. Y. Santiago, Y. Katagiri, and H. M. Geller, *J. Neurochem.* **120**, 1117 (2012).
- [62] A. R. Ketschek, S. L. Jones, and G. Gallo, *Devel. Neurobiol.* **67**, 1305 (2007).
- [63] M. A. Holland, K. E. Miller, and E. Kuhl, *Ann. Biomed. Eng.* **43**, 1640 (2015).
- [64] J. Prost, F. Jülicher, and J. Joanny, *Nat. Phys.* **11**, 111 (2015).
- [65] P. C. Bressloff and E. Levien, *Phys. Rev. Lett.* **114**, 168101 (2015).
- [66] P. Recho, T. Putelat, and L. Truskinovsky, *Phys. Rev. Lett.* **111**, 108102 (2013).
- [67] K. Tawada and K. Sekimoto, *J. Theor. Biol.* **150**, 193 (1991).
- [68] K. Kruse, J.-F. Joanny, F. Jülicher, J. Prost, and K. Sekimoto, *Eur. Phys. J. E* **16**, 5 (2005).
- [69] E. Hannezo, B. Dong, P. Recho, J.-F. Joanny, and S. Hayashi, *Proc. Natl. Acad. Sci. USA* **112**, 8620 (2015).
- [70] C. Tomba, C. Braini, B. Wu, N. S. Gov, and C. Villard, *Soft Matter* **10**, 2381 (2014).
- [71] A. Carlsson, *New J. Phys.* **13**, 073009 (2011).
- [72] P. Recho and L. Truskinovsky, *Math. Mech. Solids* (to be published).
- [73] P. Recho, T. Putelat, and L. Truskinovsky, *J. Mech. Phys. Solids* **84**, 469 (2015).
- [74] K. Xu, G. Zhong, and X. Zhuang, *Science* **339**, 452 (2013).
- [75] D. E. Moulton, T. Lessinnes, and A. Goriely, *J. Mech. Phys. Solids* **61**, 398 (2012).
- [76] B. Rubinstein, M. F. Fournier, K. Jacobson, A. B. Verkhovskiy, and A. Mogilner, *Biophys. J.* **97**, 1853 (2009).
- [77] P. Recho and L. Truskinovsky, *Phys. Rev. E* **87**, 022720 (2013).
- [78] H. Jiang and S. X. Sun, *Biophys. J.* **105**, 609 (2013).
- [79] T. H. Hui, Z. L. Zhou, J. Qian, Y. Lin, A. H. W. Ngan, and H. Gao, *Phys. Rev. Lett.* **113**, 118101 (2014).
- [80] P. Recho, J.-F. Joanny, and L. Truskinovsky, *Phys. Rev. Lett.* **112**, 218101 (2014).
- [81] W. A. Sayyad, L. Amin, P. Fabris, E. Ercolani, and V. Torre, *Sci. Rep.* **5**, 7842 (2015).
- [82] P. C. Letourneau and A. H. Ressler, *J. Cell Biol.* **98**, 1355 (1984).
- [83] J. Bamberg, D. Bray, and K. Chapman, *Nature (London)* **321**, 788 (1986).
- [84] H. Witte, D. Neukirchen, and F. Bradke, *J. Cell Biol.* **180**, 619 (2008).
- [85] F. Hellal, A. Hurtado, J. Ruschel, K. C. Flynn, C. J. Laskowski, M. Umlauf, L. C. Kapitein, D. Strikis, V. Lemmon, J. Bixby *et al.*, *Science* **331**, 928 (2011).
- [86] I. Lelidis and J.-F. Joanny, *Soft Matter* **9**, 11120 (2013).
- [87] P. A. Pullarkat, P. Dommersnes, P. Fernández, J.-F. Joanny, and A. Ott, *Phys. Rev. Lett.* **96**, 048104 (2006).
- [88] R. LeVeque, *Finite Volume Methods for Hyperbolic Problems* (Cambridge University Press, Cambridge, 2002).